Quadratic Description of Conical Intersections: Characterization of Critical Points on the Extended Seam

Fabrizio Sicilia,[‡] Lluís Blancafort,[†] Michael J. Bearpark,[‡] and Michael A. Robb*[,‡]

Department of Chemistry, Imperial College, London SW7 2AZ, United Kingdom, and Institut de Quimica Computational and Departament de Quimica, Universitat de Girona, E-17071 Girona, Spain

Received: November 16, 2006; In Final Form: January 5, 2007

In this paper, we present a practical approach for the characterization of critical points on conical intersection seams as either local minima or saddle points using second-derivative technology. The utility of this methodology is illustrated by the analysis of seven S_0/S_1 ($2A_g/1A_g$) conical intersection points involved in the photochemistry of butadiene. The characterization of critical points on the crossing seam requires second derivatives computed in curvilinear coordinates. Using such coordinates, we can represent the branching space and the intersection space to second order. Although these curvilinear coordinates are conceptually important, they also give rise to two additional practical applications. First, such coordinates yield information on the nature of vibrational modes that are stimulated following radiationless decay at a crossing point. Second, the second-order force field is directly comparable to experimental spectroscopic data for Jahn−Teller systems. We will illustrate the latter idea for the cyclopentadienyl radical.

1. Introduction

Nonadiabatic processes, passing through a conical intersection, involve molecular motions on more than one potential energy surface.[1−14] Such processes play a key role in the mechanisms of photochemical and photobiological nonradiative decay, that is, internal conversion. As we will discuss in detail subsequently, conical intersections are not isolated points but rather are part of an extended "seam" of molecular geometries where the energy of two states varies while preserving their degeneracy. Because of this, it is possible to find many "local" critical points on the conical intersection seam, which may be minima or saddle points. However, defining the precise meaning of terms such as "negative" direction of curvature, which are necessary to characterize a saddle point in the context of the seam, is not straightforward. Accordingly, we will introduce curvilinear coordinates (involving a nonlinear combination of rectilinear coordinates) that describe the locus of points belonging to the seam. As we will show, these coordinates are interesting in their own right because they yield additional information on the nature of vibrational modes that are stimulated following radiationless decay at a crossing point.

Our objective in this paper is to show that one can characterize the nature of conical intersections using second-derivative technology, in addition to the usual gradient-based methods. (We have presented initial less-general formulations of this method previously,[15,16] and Yarkony[17,18] has described a related approach using fitting methods, in contrast to our analytical gradient methods). We will illustrate the utility of this idea by examining S_0/S_1 ($1A_g/2A_g$) conical intersection points connected with the photochemistry of butadiene. As we will show, one can find seven optimized conical intersection geometries, of which three are local minima and the remaining four are saddle points on the crossing seam. We also illustrate that the same type of second-derivative information permits a direct connection between theory and experiment in Jahn−Teller systems.[11−12,19−22] In this case, the frequencies associated with the normal modes of the seam are the same as the experimental observed frequencies at the Jahn−Teller point, that is, the conical intersection geometry, except for the moat frequencies.

To characterize conical intersections using second-derivative technology, one needs to use curvilinear coordinates. Remarkably, as we will show, an examination of the characteristics of these curvilinear coordinates also provides useful information about the nature of vibrational modes that are stimulated on decay at a conical intersection. In butadiene, for example, we will show that at the *s-cisoid* conical intersection geometry the motion along the Z-E isomerization coordinate is stimulated by quadratic terms.

We have written this paper so that most of the conceptual aspects of the theoretical development are discussed in this introduction in a nonmathematical way with the aid of Figures 1−3. The mathematical details are then provided in a subsequent section. The reader should be able to skip such mathematical details and proceed directly to the results on a first reading. Accordingly, we now provide a brief summary of the essential concepts associated with the characterization of the extended conical intersection seam. We acknowledge that many of the ideas associated with the representation of conical intersection to the second order have been discussed in various places in literature (see for example refs 9−13 and 15−23).

Current practical applications and practical studies of conical intersections for photochemical mechanisms use a *first-order description*, that is, based upon gradients only. This yields the familiar schematic picture of a conical intersection shown in Figure 1. In this picture, the degeneracy at the apex of the cone is lifted in the two-dimensional subspace often referred to as the branching space[24] or g-h plane.[9−10] The branching plane is spanned by the gradient difference vector ($\bar{Q}_{x_1}$ in Figure 1) and the nonadiabatic interstate coupling vector ($\bar{Q}_{x_2}$ in Figure 1). Orthogonal to the branching plane, there exists a complementary

* Corresponding author. E-mail: mike.robb@imperial.ac.uk.
† Universitat de Girona.
‡ Imperial College.

10.1021/jp067614w CCC: $37.00
Published on Web 02/28/2007

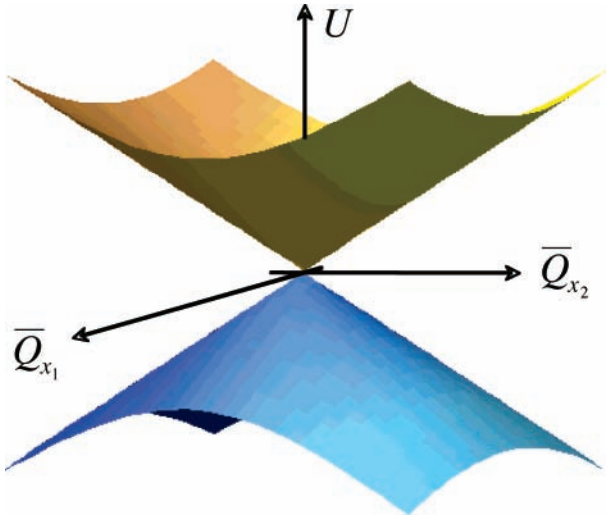

Figure 1. Double-cone topology for a conical intersection of two potential energy surfaces in the branching plane.

subspace of dimension $(3N - 8)$, where N is the number of atoms. In this subspace, called the intersection space[24] or seam space,[9−10] the energies of the two crossing states remain degenerate to first order,[7,10,23,24] that is, for an infinitesimal displacement along the rectilinear intersection-space coordinates. The branching-space and intersection-space vectors are determined in computations using gradient technology (see for example refs 7, 10, 13, 25, and 26 and references therein) and thus we refer to this as the *first-order approximation*.

A conical intersection point, that is, the apex in Figure 1, is not isolated but rather belongs to a $(3N - 8)$ crossing hyperline, that is, the intersection space.[24] This extended crossing seam can be visualized by plotting the intersecting potential energy surfaces in a space consisting of one vector from the branching plane, $\bar{Q}_{x_{1(2)}}$, and one vector from the intersection space, $\bar{Q}_i$ as shown in Figure 2. The branching space and the double-cone picture (Figure 1) remain valid as one moves along the crossing seam (Figure 2). However, the energy at the apex of the cone in Figure 1 obviously changes. The accessibility of extended portions of the conical intersection seam has proven to be an essential mechanistic feature in the photochemistry of several systems (see for example refs 1, 2, 4−8, and 27−29). Thus, a detailed description of the extended nature of the conical intersection seam is important in photochemical mechanisms and dynamics.

In Figure 2, the optimized conical intersection geometry is positioned at the origin. At this point, the gradient in the intersection subspace is zero and the two crossing states are degenerate. In contrast, within the branching plane the two states are degenerate only at the apex of the cone (the origin of the reference system in Figure 1) but the gradients are not zero. Furthermore, in Figure 2 we can see that the two states are degenerate for all values of $\bar{Q}_i$, but as we will see, this is an artifact of the first-order approximation.

Along the crossing seam (Figure 2), an optimized conical intersection can be characterized as either a minimum (Figure 2a) or a saddle point (Figure 2b) with respect to the $\bar{Q}_i$ coordinate. In the case of a saddle point, if one were to "follow the seam" (outside of the region shown in Figure 2b) then one would encounter other critical points on the crossing seam at lower energy.[15,16] However, currently available methods for studying conical intersections are based on gradient technology alone[10,26,30−32] and thus one cannot currently characterize the optimized crossing point as either a minimum (Figure 2a) or a saddle point (Figure 2b). It should be clear that a method for the determination of the curvature at a crossing point would have many practical applications. However, the coordinates used to describe the branching space (and the intersection space) need to be generalized in order to determine the curvature of the conical intersection seam energy. We now discuss this point briefly.

We begin by explaining why the coordinates used in the description of the conical intersection need to be generalized in order to characterize the curvature of the seam energy. In Figure 2, there is a simplification that arises from the first-order, that is, gradient-based description of conical intersections, that does not occur at higher order. In Figure 2, one can see that the extended seam is parallel to the intersection coordinate, $\bar{Q}_i$, that is, the seam curve lies in the plane of the energy and the chosen intersection-space coordinate. However, in numerical computations[15−18] one finds that the degeneracy is, in practice, lifted for a finite displacement along any intersection coordinate (Figure 3c and d). Thus, beyond first order, the intersection space as described in rectilinear coordinates is like a Renner−Teller intersection of two degenerate states of a linear molecule (see for example ref 33). Although this seems inconsistent at first, in fact, such degeneracy lifting is just a manifestation of the assumption (made within the first-order description) that the seam lies in the energy/intersection coordinate plane. In general, the crossing seam is curved[9,10,13,15,18,24] as shown in Figure 3a and b, which is analogous to Figure 2a and b in the first-order approximation. This provides the reason for a more general choice of coordinate system in order to describe the curvature of the seam energy.

We now discuss Figure 3, which shows the crossing seam including the quadratic effects. Figure 3a (minimum) and b (saddle point) is analogous to Figure 2a and b. The line f_i corresponds to the projection of the seam $U(f_i)$ on the coordinate space consisting of one coordinate from the branching plane, $\bar{Q}_{x_{12}}$, and one from the intersection space, $\bar{Q}_i$. In Figure 2, f_i would be coincident with $\bar{Q}_i$. Thus, the major difference from Figure 2 is that the crossing seam has become *curved* in Figure 3. By curved we mean that the seam bends toward the branching plane coordinate, with a mixing of branching-space and intersection-space coordinates.[15−18] This curvature is required to describe finite displacements where the degeneracy is preserved.[15,16]

In Figure 3c and d we show cuts through Figure 3a and b in the $(U, \bar{Q}_i)$ plane, corresponding to Figure 2c and d. It is clear in this figure that the two potential energy surfaces split apart (Figure 3c and d) along any finite displacement lying strictly along the rectilinear first-order intersection modes, $\bar{Q}_i$, that is, in the plane containing energy and the intersection coordinate.

Figure 3 also shows that a curvilinear coordinate is essential to describe the behavior of the extended seam. If we define the curvilinear coordinates as f_i, then the crossing seam energy can be written as a function of these $(3N - 8)$ variables $U(f_i)$ rather than the $(3N - 6)$ rectilinear coordinates. It then becomes clear that the curvature of the seam energy becomes simply the second derivative of the seam energy with respect to such curvilinear coordinates.[15,16] We will refer to the matrix of second derivatives computed in this way as the *intersection-space Hessian*.

The curvilinear coordinates just discussed are the second-order generalization of the intersection adapted coordinates introduced by Atchity et al.[24] Following their original definition, the $(3N - 8)$ degeneracy maintaining curvilinear coordinates span the quadratic intersection subspace, whereas the remaining two coordinates define the quadratic branching subspace. We used the term quadratic intersection-space subspace to describe

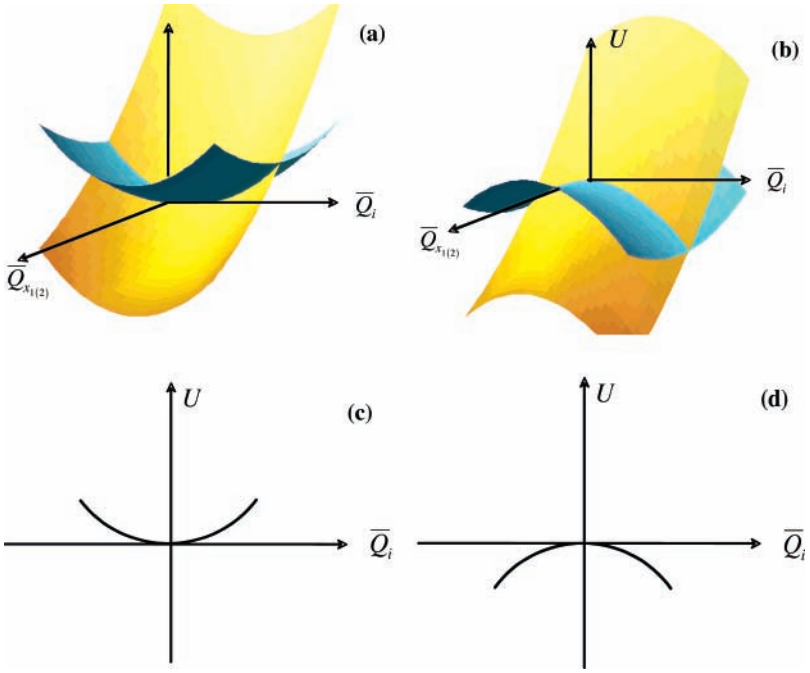

Figure 2. Schematic representation of the two crossing potential energy surfaces in a space consisting of one coordinate belonging to the branching space and one coordinate belonging to the intersection-space: (a) minimum, (b) saddle point, (c) cross section of a along the intersection coordinate, $\bar{Q}_i$, and (d) cross section of b along the intersection coordinate, $\bar{Q}_i$.

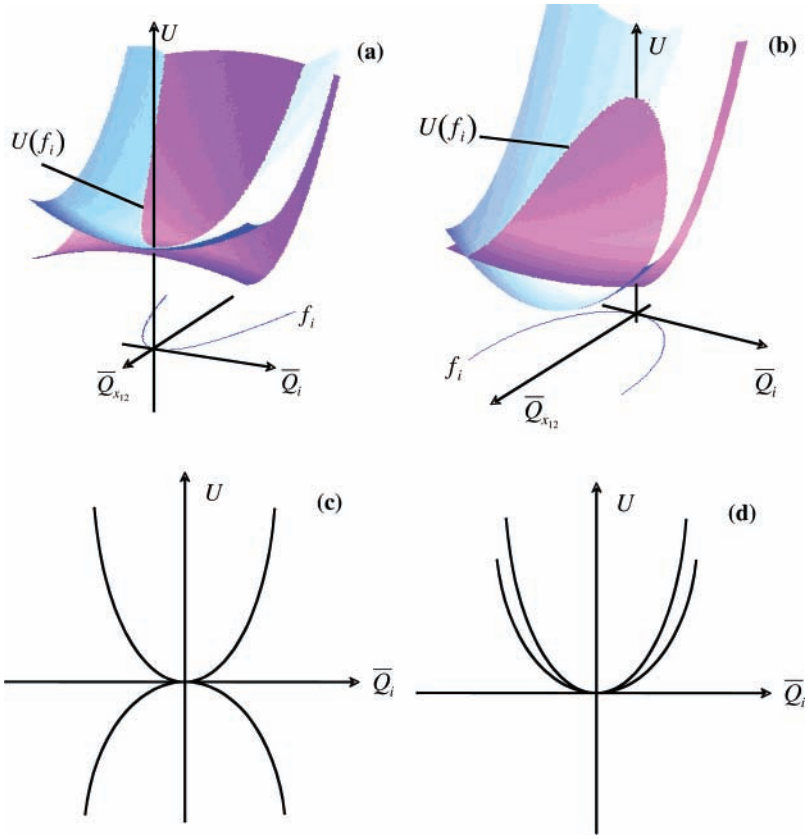

Figure 3. Locus of the conical intersection seam $U(f_i)$ and the corresponding curvilinear coordinate f_i: (a) minimum, (b) saddle point, (c) cross section of a along first-order intersection-space coordinate $\bar{Q}_i$, and (d) cross section of b along first-order intersection-space coordinate, $\bar{Q}_i$.

the situation where the degeneracy is preserved for any displacement along the corresponding curvilinear coordinates correct to second-order. Because of this definition, we can describe the curvature of the conical intersection seam in this curvilinear coordinate space. The quadratic branching space is defined analogously using the branching-space curvilinear coordinates. The picture given in Figure 1 remains valid; however, the axes in this case become curved. As we will discuss subsequently, the curvature of this space, obtained by mixing first-order branching space and first-order intersection

space,[15−18] is important for discussing the dynamics at conical intersections.

In a subsequent illustrative application to the photochemistry of butadiene, we will locate several conical intersection points, for which the gradient is zero within the $(3N - 8)$ intersection space. Then using the intersection-space Hessian, we will characterize such critical points on the $(3N - 8)$ crossing hyperline as minima (Figure 3a) or saddle points (Figure 3b). Moreover, we will show how one can carry out a normal-mode analysis at a saddle point on the seam. The normal mode associated with an imaginary frequency will be associated with a particular intersection-space curvilinear coordinate and can be used to predict the occurrence of new conical intersection geometries at lower energy.

We will also show how the second-derivative analysis developed for conical intersections can be used for the study of symmetry-induced crossing occurring in Jahn−Teller active molecules.[11,19−22,35] The important point is that the seam frequencies evaluated with our second-derivative methodology can be compared directly with spectroscopic frequencies and the seam normal modes can be used in place of the normal modes of the distorted molecule. In addition, the linear and quadratic potential energy constants evaluated at an optimized conical intersection point can be applied directly as parameters in the force field used to simulate recorded spectra[19−22,36,37] or to perform dynamics studies.[11,12,35,38] We will discuss such an application in the analysis of the cyclopentadienyl radical conical intersection, where we will show that calculated and experimental frequencies agree to within a few percent.

2. Theory

We begin this section by introducing a set of rectilinear coordinates that are suitable for the description of conical intersections. Using the notation introduced previously,[15] such coordinates can be defined as

$$\bar{Q} = (\bar{Q}_{x_1}, \bar{Q}_{x_2}) \oplus (\bar{Q}_3, \bar{Q}_4, ..., \bar{Q}_{3N-6}) \tag{1}$$

The first parentheses contain the two coordinates necessary to describe the first-order branching space and the second correspond to the $(3N - 8)$ coordinates spanning the first-order intersection space. The two coordinates spanning the branching space are the gradient difference (eq 2a) and the interstate coupling (eq 2b) vectors.

$$x_1^{(i\gamma)} = \frac{\partial(E_B - E_A)}{\partial \xi_{i\gamma}} \tag{2a}$$

$$x_2^{(i\gamma)} = \frac{\partial \langle \Psi_A | \hat{H} | \Psi_B \rangle}{\partial \xi_{i\gamma}} \tag{2b}$$

In eq 2, states A and B are the two electronic states associated with the conical intersection. $\xi_{i\gamma}$ is the γth mass-weighted Cartesian coordinate of the ith atom. The index i labels the N atoms and γ the Cartesians components, x, y and z. Although the degeneracy is linearly lifted in the branching plane, it is retained in the orthogonal $(3N - 8)$ subspace spanned by the remaining coordinates. The coordinates used in eqs 1 and 2 were originally suggested by Davidson[39] and later utilized by Atchity et al.,[24] who referred to them as *intersection-adapted coordinates*. Although Atchity et al. defined this coordinate system in a very general way, these coordinates were only used in the first-order approximation, that is, first-order intersection adapted coordinates.

We now move to discuss the two-state quadratic expansion of the potential energy using the coordinates defined in eqs 1 and 2. The type of expansion we will use has been applied extensively in the study of Jahn−Teller systems.[11,12,19−22,38] However, in the present work we will use the coordinates defined in eqs 1 and 2, whereas in Jahn−Teller studies, the normal coordinates of a reference system at a minimum configuration are normally utilized.

Assuming that A and B are two coupled electronic states, the two-state potential energy matrix can be constructed as a Taylor expansion about the crossing point. Diagonalization of the two-by-two potential energy matrices yields the adiabatic energies for any displacements of the $\bar{Q}_i$ defined in eq 1. This expansion can be expressed in rectilinear first-order intersection adapted coordinates and truncated at the second order as shown in eq 3:

$$\mathbf{W}(\bar{\mathbf{Q}}) = \mathbf{W}^{(0)} + \mathbf{W}^{(1)}(\bar{\mathbf{Q}}) + \frac{1}{2}\mathbf{W}^{(2)}(\bar{\mathbf{Q}}) \tag{3}$$

In eq 3, the zero-order term, $\mathbf{W}^{(0)}$, is a diagonal matrix where each element corresponds to the energy of the two degenerate states, E_A and E_B, evaluated at the reference crossing point, $\bar{\mathbf{Q}}_0$:

$$\mathbf{W}^{(0)} = \frac{E_A + E_B}{2}\mathbf{1} + \begin{pmatrix} -\frac{E_B - E_A}{2} & 0 \\ 0 & \frac{E_B - E_A}{2} \end{pmatrix} \tag{4}$$

1 represents the identity matrix. It should also be noticed that E_A and E_B are equal because the expansion is performed around a crossing point. This value can then be taken as reference point and $\mathbf{W}^{(0)}$ set to zero. In eq 4, we have chosen to do the expansion relative to $(E_A + E_B)/2$ and $(E_B - E_A)/2$ because, as we will show subsequently, the conditions for the seam are most conveniently expressed as combinations of derivatives of the sum and the difference of the state energies.

The first-order potential energy matrix has the form

$$\mathbf{W}^{(1)} = \left(\frac{\lambda_1}{2}\bar{Q}_{x_1} + \frac{\lambda_2}{2}\bar{Q}_{x_2}\right)\mathbf{1} + \begin{pmatrix} -\frac{\delta\kappa}{2}\bar{Q}_{x_1} & \kappa^{AB}\bar{Q}_{x_2} \\ \kappa^{AB}\bar{Q}_{x_2} & \frac{\delta\kappa}{2}\bar{Q}_{x_1} \end{pmatrix} \tag{5}$$

The linear potential constants used in eq 5 are defined as

$$\delta\kappa \equiv \left.\frac{\partial(E_B - E_A)}{\partial \bar{Q}_{x_1}}\right|_0 \tag{6a}$$

$$\kappa^{AB} \equiv \left.\frac{\partial \langle \Psi_A | \hat{H} | \Psi_B \rangle}{\partial \bar{Q}_{x_2}}\right|_0 \tag{6b}$$

$$\lambda_i \equiv \left.\frac{\partial(E_A + E_B)}{\partial \bar{Q}_{x_i}}\right|_0 \quad i = x_1, x_2 \tag{6c}$$

The subscript 0 indicates that these quantities are evaluated at the conical intersection point. It should be noticed that all of the gradient components are limited to the branching plane, $\bar{Q}_{x_1}$ and $\bar{Q}_{x_2}$, because the expansion was performed around an optimized conical intersection point.

We now discuss the quadratic term in the expansion of the potential energy matrix (eq 3). For simplicity, the quadratic term will be divided in three parts: $\mathbf{W}_a^{(2)}$ the contribution arising within the branching plane (eq 7a), $\mathbf{W}_b^{(2)}$ the contributions within the intersection space (eq 7b), and $\mathbf{W}_c^{(2)}$ the contributions from the coupling of modes belonging to both subspaces (eq 7c).

$$\mathbf{W}_a^{(2)} = \left(\sum_{i,j\in BS} \frac{{}^{BS}\omega_{ij}}{2}\bar{Q}_i\bar{Q}_j\right)\mathbf{1} + \begin{pmatrix} -\sum_{i,j\in BS}\frac{{}^{BS}\delta\gamma_{ij}}{2}\bar{Q}_i\bar{Q}_j & \sum_{i,j\in BS}{}^{BS}\eta_{ij}^{AB}\bar{Q}_i\bar{Q}_j \\ \sum_{i,j\in BS}{}^{BS}\eta_{ij}^{AB}\bar{Q}_i\bar{Q}_j & \sum_{i,j\in BS}\frac{{}^{BS}\delta\gamma_{ij}}{2}\bar{Q}_i\bar{Q}_j \end{pmatrix} \quad (7a)$$

$$\mathbf{W}_b^{(2)} = \left(\sum_{i,j\in IS} \frac{{}^{IS}\omega_{ij}}{2}\bar{Q}_i\bar{Q}_j\right)\mathbf{1} + \begin{pmatrix} -\sum_{i,j\in IS}\frac{{}^{IS}\delta\gamma_{ij}}{2}\bar{Q}_i\bar{Q}_j & \sum_{i,j\in IS}{}^{IS}\eta_{ij}^{AB}\bar{Q}_i\bar{Q}_j \\ \sum_{i,j\in IS}{}^{BS}\eta_{ij}^{AB}\bar{Q}_i\bar{Q}_j & \sum_{i,j\in IS}\frac{{}^{IS}\delta\gamma_{ij}}{2}\bar{Q}_i\bar{Q}_j \end{pmatrix} \quad (7b)$$

$$\mathbf{W}_c^{(2)} = \left(\sum_{i\in BS,\, j\in IS} \frac{{}^{BS/IS}\omega_{ij}}{2}\bar{Q}_i\bar{Q}_j\right)\mathbf{1} + \begin{pmatrix} -\sum_{i\in BS,j\in IS}\frac{{}^{BS/IS}\delta\gamma_{ij}}{2}\bar{Q}_i\bar{Q}_j & \sum_{i\in BS,j\in IS}{}^{BS/IS}\eta_{ij}^{AB}\bar{Q}_i\bar{Q}_j \\ \sum_{i\in BS,j\in IS}{}^{BS/IS}\eta_{ij}^{AB}\bar{Q}_i\bar{Q}_j & \sum_{i\in BS,j\in IS}\frac{{}^{BS/IS}\delta\gamma_{ij}}{2}\bar{Q}_i\bar{Q}_j \end{pmatrix} \quad (7c)$$

The quadratic potential energy constants in eq 7 are defined as

$$\omega_{ij} \equiv \left.\frac{\partial^2(E_A+E_B)}{\partial\bar{Q}_i\,\partial\bar{Q}_j}\right|_0 \quad (8a)$$

$$\eta_{ij}^{AB} \equiv \left.\frac{\partial^2\langle\Psi_A|\hat{H}|\Psi_B\rangle}{\partial\bar{Q}_i\,\partial\bar{Q}_j}\right|_0 \quad (8b)$$

$$\delta\gamma_{ij} \equiv \left.\frac{\partial^2(E_B-E_A)}{\partial\bar{Q}_i\,\partial\bar{Q}_j}\right|_0 \quad (8c)$$

All of these quantities are computed using the state-averaged Hessian for each individual state, which can be analytically determined for CASSCF wavefunctions.[40,41]

Now our objective is to analytically define the curvilinear coordinates (Figure 3) that give the locus of the seam of intersection. We can then formulate the equation for the Hessian in the intersection space correct to second order. As we will show, this matrix can be used for the characterization of optimized conical intersection structures.

The diagonalization of the potential energy matrix to second order defined in eq 3 provides the analytical expansion of each of the two intersecting potential energy surfaces:

$$U_{A,B} = \frac{1}{2}\left\{\sum_{i\in BS}\lambda_i\bar{Q}_i + \sum_{i,j=1}^{3N-6}\frac{\omega_{ij}}{2}\bar{Q}_i\bar{Q}_j\right\} \pm \frac{1}{2}\sqrt{\left[\delta\kappa\bar{Q}_{x_1} + \sum_{i,j=1}^{3N-6}\frac{\delta\gamma_{ij}}{2}\bar{Q}_i\bar{Q}_j\right]^2 + 4\left[\kappa^{AB}\bar{Q}_{x_2} + \sum_{i,j=1}^{3N-6}\frac{\eta_{ij}^{AB}}{2}\bar{Q}_i\bar{Q}_j\right]^2} \quad (9)$$

In the following development we neglect the terms $\mathbf{W}_a^{(2)}$ (eq 7a) and $\mathbf{W}_c^{(2)}$ (eq 7c), retaining only the terms involving the intersection space alone, $\mathbf{W}_b^{(2)}$ (eq 7b), because we are interested in the curvature of the seam energy. We refer to this simplification as the *parabolic approximation*, shown in Figure 3a and b. We have carried through the analysis without neglecting $\mathbf{W}_a^{(2)}$ (eq 7a) and $\mathbf{W}_c^{(2)}$ (eq 7c) and it does not seem possible to parametrize the seam (as discussed below) for this general situation. However, the curvatures computed at the point of intersection will be the same. Although the inclusion of the neglected terms would allow the seam to be described over a more extended region, it would complicate the mathematical derivation and would not yield additional insight.

Setting the quantity in the square root to zero (eq 9) and neglecting $\mathbf{W}_a^{(2)}$ (eq 7a) and $\mathbf{W}_c^{(2)}$ (eq 7c) yields the following conditions to be satisfied by our curvilinear coordinates:

$$\begin{cases} \delta\kappa\bar{Q}_{x_1} + \sum_{i,j\in IS}\frac{{}^{IS}\delta\gamma_{ij}}{2}\bar{Q}_i\bar{Q}_j = 0 \\ \kappa^{AB}\bar{Q}_{x_2} + \sum_{i,j\in IS}\frac{{}^{IS}\eta_{ij}^{AB}}{2}\bar{Q}_i\bar{Q}_j = 0 \end{cases} \quad (10)$$

The conditions given by eq 10 define the parametrized *parabolic intersection coordinates*, f_i. Such parabolic coordinates can be chosen as

$$\bar{Q}_{x_1} = \sum_{i,j=3}^{3N-6}\alpha_{ij}f_if_j \qquad \alpha_{ij} = -\frac{{}^{IS}\delta\gamma_{ij}}{2\delta\kappa} \quad (11a)$$

$$\bar{Q}_{x_2} = \sum_{i,j=3}^{3N-6}\mu_{ij}f_if_j \qquad \mu_{ij} = -\frac{{}^{IS}\eta_{ij}^{AB}}{2\kappa_{AB}} \quad (11b)$$

$$\bar{Q}_i = \beta_i f_i \qquad \beta_i = 1 \quad (11c)$$

In other words, for any displacement along f_i (eq 11), eq 10 remains satisfied and the degeneracy is retained correct to second order. The particular form of eq 11, among many possible, was chosen so that the scale factors,[42] which are essential in the differentiation with respect to curvilinear coordinates, were unity.

We can write the expression for the seam energy as function of the curvilinear coordinates f_i, (eq 11), as

$$U_{Seam} = \sum_{i,j\in IS}\frac{\lambda_{x_1}}{2}(\alpha_{ij}f_if_j) + \frac{\lambda_{x_2}}{2}(\mu_{ij}f_if_j) + \frac{{}^{IS}\omega_{ij}}{4}\beta_i\beta_jf_if_j \quad (12)$$

Because the expansion was performed at an optimized point, the gradient of the seam energy within the intersection space is necessarily zero and the curvature of the seam energy is given simply by its second derivative, which can be written as

$$\frac{\partial^2 U_{Seam}}{\partial f_k \partial f_l} = \lambda_{x_1}\alpha_{kl} + \lambda_{x_2}\mu_{kl} + \frac{^{IS}\omega_{kl}}{2}\beta_k\beta_l \qquad (13)$$

In eq 13, the indices k and l run over the $(3N-8)$ intersection-space curvilinear coordinates. Inserting the constants defined in eq 11, we obtain the *intersection-space Hessian*:

$$\frac{\partial^2 U_{Seam}}{\partial f_k \partial f_l} = \frac{1}{2}\left(^{IS}\omega_{ij} - \frac{\lambda_{x_1}}{\delta\kappa}\,^{IS}\delta\gamma_{ij} - \frac{\lambda_{x_2}}{\kappa^{AB}}\,^{IS}\eta_{ij}^{AB}\right) \qquad (14)$$

The diagonalization of the intersection-space Hessian provides the curvature of the energy seam and a set of eigenvectors, which are the tangent vectors to the curvilinear intersection-space coordinates, f_i. Throughout the development, both gradient difference, $\delta\kappa$, and interstate coupling, κ^{AB}, are assumed to have nonzero length. However at a singlet−triplet crossing, where the κ^{AB} and η^{AB} terms are zero, the definition of the intersection-space Hessian is simply obtained by leaving out the terms including these constants from eq 14.

We conclude this section with a discussion of the branching-space curvilinear coordinates that are complementary to the intersection-space coordinates used in the previous discussion of the crossing seam. The two parabolic branching-space coordinates are defined as (eqs 2.13.a and 2.13.b of ref 24)

$$f_1 = \delta\kappa\bar{Q}_{x_1} + \sum_{i,j=3}^{3N-6}\frac{^{IS}\delta\gamma_{ij}}{2}\bar{Q}_i\bar{Q}_j \qquad (15a)$$

$$f_2 = \kappa^{AB}\bar{Q}_{x_2} + \sum_{i,j=3}^{3N-6}\frac{^{IS}\eta_{ij}^{AB}}{2}\bar{Q}_i\bar{Q}_j \qquad (15b)$$

When the two potential energy surfaces (eq 9) are expressed as functions of the two branching-space coordinates (eq 15), one retains the simple double-cone picture shown in Figure 1 corrected to second-order:

$$U_{A,B} = \bar{H}(f_{x_1}, f_{x_2}) \pm \sqrt{f_{x_1}^2 + f_{x_2}^2} \qquad (16)$$

Thus, the degeneracy is lifted along f_1 and f_2 (eq 16), that is, the branching-space coordinates, and retains along the remaining $f_3, f_4, \ldots, f_{3N-6}$ (eq 11), that is, intersection-space coordinates.

It can be seen in eqs 15a and b that the first-order branching-space coordinates, that is, gradient difference, $\bar{Q}_{x_1}$ (eq 2a), and nonadiabatic interstate coupling vector, $\bar{Q}_{x_2}$ (eq 2b), mix with the intersection-space coordinates quadratically via the mixing coefficients $\delta\gamma_{ij}$ and η_{ij}^{AB}, giving rise to curvilinear coordinates. Thus, one can examine the contributions of various first-order intersection-space motions by diagonalization of the $\delta\gamma_{ij}$ and η_{ij}^{AB} matrices. The largest eigenvalues will correspond to the strongest mixing modes.

Using these coordinates, one retains the simple double-cone picture shown in Figure 1 corrected to second order (eq 16). Thus, it is expected that the modes that make the dominant contribution to the coordinates f_1 and f_2 (eq 15) will become populated after photochemical decay, in addition to the population of the first-order branching-space modes. A trajectory passing through a surface hop will have momentum in those coordinates populated during evolution on the excited states. At the surface hop, additional momentum will be generated in branching-space modes and those modes that have large second-order couplings (eq 15), as determined by the eigenvalues of the $\delta\gamma_{ij}$ and η_{ij} matrices.

3. Computational Details

All of the conical intersections were computed using the *complete active space self-consistent field* (CASSCF) method implemented in a development version of Gaussian.[43] The active space of four π electrons and four π orbitals and a 6-31G* basis set was used to optimize the butadiene conical intersections. For the cyclopentadienyl radical, five π electrons and five π orbitals were used with Dunning's cc-pVDZ basis set.

All of the conical intersection structures were located using the algorithm of Bearpark et al.[32] and using state-averaged wavefunctions for the equally weighted ground and first excited states (other conical intersection optimization methods have now been developed in addition to ref 32 and the original algorithm of Yarkony,[44] see for example refs 24, 30, and 31).

All of the quantities needed to characterize critical points on the extended conical intersection seam (defined above in section 2) can now be computed analytically. The linear potential energy constants (eq 6) are evaluated during a standard conical intersection optimization: $\delta\kappa$ and κ^{AB}, respectively, are the length of the gradient difference and interstate coupling vectors, λ_i is the sum of the gradient projections onto the gradient difference ($i = x_1$) and the interstate coupling direction ($i = x_2$). In all of our calculations, the nonadiabatic interstate coupling vector was orthogonalized to the gradient difference vector.

In the second-order potential matrices (eq 7), there are three types of potential energy constants to be evaluated, two diagonal ($\delta\gamma_{ij}$ eq 8c, ω_{ij} eq 8a) and one off-diagonal (η_{ij}^{AB} eq 8b). The diagonal terms are computed using a specific combination of the projected state-averaged (SA) Hessians of the two electronic states. The SA Hessians for the two states are analytically computed as discussed in refs 40 and 41. The intersection-space SA Hessians are obtained using an extension of a method proposed to calculate frequencies orthogonal to a reaction path as shown in ref 15. The *second-order interstate coupling terms*, η_{ij}^{AB}, have been computed using a combination of the two wavefunctions ϕ_A and ϕ_B optimized at the conical intersection geometry:

$$\phi_\pm = \frac{1}{\sqrt{2}}(\phi_A \pm \phi_B) \qquad (17)$$

The elements of the Hessian for these two rotated states, $\gamma_{ij}^{\pm}$, can be expressed in terms of the original ones:

$$\gamma_{ij}^{\pm} = \frac{1}{2}[\omega_{ij} \pm 2\eta_{ij}^{AB}] \qquad (18)$$

The elements ω_{ij} and η_{ij}^{AB} are defined in eq 8. From eq 18, the η_{ij}^{AB} can be computed easily. Thus, the second-order potential energy constants defined in eq 8 are computed using the various combinations of the SA Hessians of the two intersecting states projected onto the intersection space. We have implemented our approach within the CASSCF approximation; however, the same formalism can, in principle, be implemented in other higher level theoretical approaches provided the necessary Hessians can be computed.

SCHEME 1: Photochemistry of Butadiene

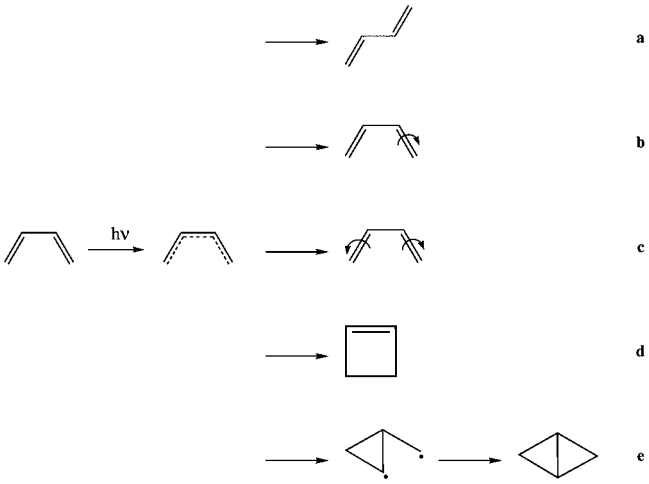

Finally, a comment on accuracy seems relevant at this stage. We have implemented our analysis at the CASSCF level. This requires state-averaged Hessians and it seems unlikely that one could implement such Hessian computations at a higher level of theory such as CASPT2. Nevertheless, it is well known that gradients and frequencies of nonionic states are often well reproduced at levels of theory that do not include dynamic correlation. Thus, we expect that our results for the Jahn−Teller Hamiltonian, where direct comparison with experiment is possible, should have an agreement within 10% like SCF frequencies. In fact, as we will see, our agreement for the Jahn−Teller frequencies in the cyclopentadienyl radical is not quite so accurate. However, the remaining error is predicted as a consequence of neglecting the coupling terms between the branching-space and intersection-space vectors.

4. Results and Discussion

It is our intention in this section to illustrate the utility of the methodology presented in sections 1 and 2. We shall use the photochemistry of butadiene to show how one can characterize the topology of the S_0/S_1 intersection seam and how qualitative dynamics information can be obtained from the analysis of the nature of branching-space curvilinear coordinates (eqs 15a and b). We shall also show how the potential constants obtained in the analysis of the seam can be used in the study of the Jahn−Teller active cyclopentadienyl radical system. Here, the seam frequencies evaluated with our methodology can be compared directly with spectroscopic data.

Example 1: The $S_0/S_1(^1A_g)$ Conical Intersection Hyperline of Butadiene. Over the years, butadiene photochemistry has stimulated many theoretical studies.[1,2,4,5,7,14,29,44−47] Experiments performed on butadiene in dilute solution had shown that irradiation with a 254-nm light source leads to a *s-cis/s-trans* isomerization (Scheme 1a), double-bond isomerizations (Scheme 1b and c), and cyclobutene (Scheme 1d), bicyclo [1.1.0] butane, and methylenecyclopropyl 1,3-diradical formation[44] (Scheme 1e). Over a decade ago, a ^1A_g photochemical pathway involving a passage through a conical intersection was proposed.[46] In that early CASSCF study, three conical intersection geometries were located on the intersection seam between the ground (S_0) and first excited state (S_1): a *s-cisoid*, a *s-transoid*, and a *central* conical intersection geometry. The *s-cisoid* structure was assumed to be the starting point for the generation of the photochemical products for *cis−trans* isomerization (Scheme 1a), *Z-E* isomerization (Scheme 1b), *Z,Z-E,E* isomerization (Scheme 1c), and cyclobutene (Scheme 1d) and bicyclo[1,1,0] butane formation (Scheme 1e). Indeed, in subsequent work[5,48] ground-state reaction paths leading to many of these products were located. Within the intersection space, the *central* conical intersection was assumed to be a saddle point between the *s-cisoid* and *s-transoid* conical intersection structures.

TABLE 1: Important Geometric Parameters for the Optimized Butadiene CI Geometries[a]

Geometry[b]	1-2	2-3	3-4	1-2-3	2-3-4	1-2-3-4	7-2-3-8
$\mathbf{CI_{cis}}$	1.46	1.40	1.47	90.39	121.56	52.61	4.19
$\mathbf{CI_{ring}}$	1.46	1.75	1.42	54.79	112.70	114.84	6.53
$\mathbf{CI_{trans}}$	1.47	1.43	1.46	120.09	99.47	118.45	168.22
$^{SP}\mathbf{CI_{trans/trans}}$	1.46	1.47	1.46	107.52	107.52	94.82	162.02
$^{SP}\mathbf{CI_{cis/cis}}$	1.48	1.44	1.48	109.22	109.22	86.57	41.44
$^{SP}\mathbf{CI_{cis/trans}}$	1.47	1.50	1.47	123.66	123.66	107.94	71.61
$^{SP}\mathbf{CI_{cis/ring}}$	1.41	1.53	1.36	76.44	119.24	85.63	24.25

[a] The bond lengths are expressed in angstroms, and the angles are presented in degrees. [b] Full Cartesian coordinates for all of the geometries are given in the Supporting Information (Table S7).

We have now exhaustively searched for all possible low-energy critical points on the S_0/S_1 ($1A_g/2A_g$) crossing seam of butadiene. We have found three minima, $\mathbf{CI_{cis}}$, $\mathbf{CI_{trans}}$, and $\mathbf{CI_{ring}}$, and four saddle points, $^{SP}\mathbf{CI_{cis/cis}}$, $^{SP}\mathbf{CI_{trans/trans}}$, $^{SP}\mathbf{CI_{cis/trans}}$, and $^{SP}\mathbf{CI_{cis/ring}}$. The corresponding geometries and energetics are collected in Tables 1 and S1 (Table S1 is available in the Supporting Information, where the Cartesian coordinates of all of the optimized structures are also provided in Table S7). In Table 1, there are two $\mathbf{CI_{cis}}$ conical intersections that are chemically equivalent and connected by the saddle point $^{SP}\mathbf{CI_{cis/cis}}$. A similar connectivity exists between the $\mathbf{CI_{trans}}$, $^{SP}\mathbf{CI_{trans/trans}}$, and $\mathbf{CI_{trans}}$. The global relationships between these conical intersection geometries are illustrated in Figure 4. The potential contants and first-order branching plane vectors (eq 2 and Figure 1) are reported in Tables S2 and 2, respectively. The normal modes [tangent to the intersection-space curvilinear coordinates, f_i (eq 11)] associated with the imaginary frequencies at the conical intersection saddle points ($^{SP}\mathbf{CI}$) are displayed in Table 3. For example, the vector shown for the $^{SP}\mathbf{CI_{tran/trans}}$ structure is the tangent vector to the curvilinear coordinate that connects the two chemically equivalent $\mathbf{CI_{trans}}$. Here, the "kink" angles, that is, 120° angle (C1−C2−C3) and the 99° angle (C2−C3−C4), in $\mathbf{CI_{trans}}$ are interchanged to give the corresponding chemically equivalent structure, $\mathbf{CI_{trans'}}$.

It is apparent from inspection of the results presented in Table 1 and Figure 4 that the topology of the conical intersection seam is richer than that in the initial study,[46] where only *s-cisoid*, *s-transoid*, and *central* conical intersections could be located. In the region where the *central* conical intersection point was located in ref 46, we find $^{SP}\mathbf{CI_{cis/cis}}$, $^{SP}\mathbf{CI_{trans/trans}}$, and $^{SP}\mathbf{CI_{cis/trans}}$.

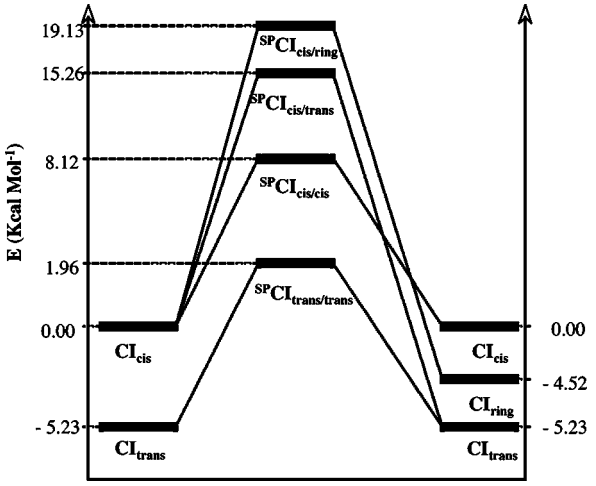

Figure 4. Schematic representation of the topology of the S_0/S_1 conical intersection seam of butadiene. The critical point geometries are given in Table 1 (**SP** = saddle point).

TABLE 2: Gradient Difference (Equation 2a) and Interstate Coupling Vectors (Equation 2b) for the Optimized Butadiene Conical Intersection Geometries

Geometry	Gradient Difference Vector	Interstate Coupling Vector
$\mathbf{CI_{cis}}$	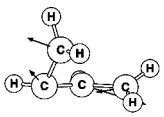	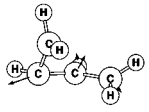
$\mathbf{CI_{ring}}$	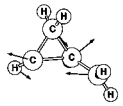	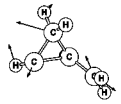
$\mathbf{CI_{trans}}$	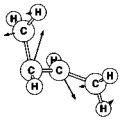	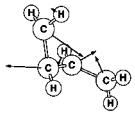
$^{SP}\mathbf{CI_{trans/trans}}$	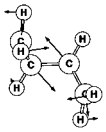	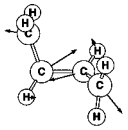
$^{SP}\mathbf{CI_{cis/cis}}$	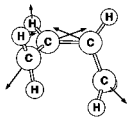	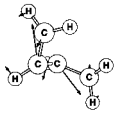
$^{SP}\mathbf{CI_{cis/trans}}$	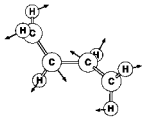	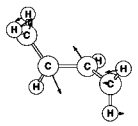
$^{SP}\mathbf{CI_{cis/ring}}$	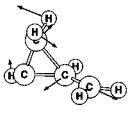	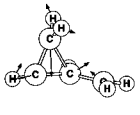

We also find a new conical intersection not documented in ref 46, $\mathbf{CI_{ring}}$, as well as $^{SP}\mathbf{CI_{cis/ring}}$, which connects $\mathbf{CI_{ring}}$ to $\mathbf{CI_{cis}}$.

We now briefly comment on the region of the intersection space originally characterized as the *central* conical intersection and now characterized by three individual saddle points on the crossing seam. The topology of this intersection-space region can be explained with the help of the imaginary seam frequencies and normal modes displayed in Table 3 for $^{SP}\mathbf{CI_{cis/cis}}$, $^{SP}\mathbf{CI_{trans/trans}}$, and $^{SP}\mathbf{CI_{cis/trans}}$. The $^{SP}\mathbf{CI_{cis/cis}}$ structure, of C_2 symmetry, connects two equivalent $\mathbf{CI_{cis}}$ structures, which differ mainly according to which of the two C−C−C angles has the characteristic kink. In a similar way, structure $^{SP}\mathbf{CI_{trans/trans}}$, also of C_2 symmetry, connects two equivalent $\mathbf{CI_{trans}}$ structures. The connection between the *s-cisoid* and *s-transoid* regions of the seam is given by $^{SP}\mathbf{CI_{cis/trans}}$. This structure also has C_2 symmetry and has one imaginary frequency of 1163 cm^{-1} with a torsion component that connects the *s-cisoid* and *s-transoid* structures. The imaginary frequency displayed in Table 3 and the branching-space vectors shown in Table 2 for $^{SP}\mathbf{CI_{cis/trans}}$ are all totally symmetric. Thus, $^{SP}\mathbf{CI_{cis/trans}}$ appears to connect the other two saddle points, $^{SP}\mathbf{CI_{cis/cis}}$ and $^{SP}\mathbf{CI_{trans/trans}}$, which have the same symmetry. Presumably the points are connected through the equivalent of valley-ridge inflection points in the intersection space. This probably explains the fact that the imaginary frequencies of $^{SP}\mathbf{CI_{cis/cis}}$ and $^{SP}\mathbf{CI_{trans/trans}}$ are not totally symmetric.

TABLE 3: Seam Normal Modes of the Conical Intersection Saddle Points

Geometry	Seam Frequency (cm^{-1})	Seam transition mode
$^{SP}\mathbf{CI_{trans/trans}}$	445.41 *i*	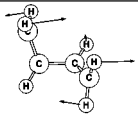
$^{SP}\mathbf{CI_{cis/cis}}$	729.17 *i*	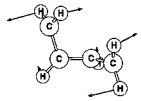
$^{SP}\mathbf{CI_{cis/trans}}$	1163.01 *i*	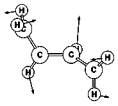
$^{SP}\mathbf{CI_{cis/ring}}$	353.22 *i*	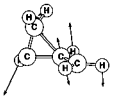

The cyclopropene-like minimum, $\mathbf{CI_{ring}}$, located for the first time in this study, deserves a brief comment. The $\mathbf{CI_{ring}}$ is connected to $\mathbf{CI_{cis}}$, discussed previously, through structure $^{SP}\mathbf{CI_{cis/ring}}$ (Table 1). In previous studies,[45,48,49] no direct ground-state reaction path was located that would lead to the methyl-enecyclopropyl 1,3-diradical intermediate (Scheme 1e). In light of this observation, one might now suggest that a ground-state reaction path from $\mathbf{CI_{ring}}$ would lead to the 1-methyl-cyclopropene intermediate (Scheme 1e), which is the precursor of the bicyclo[1,1,0] butane photoproduct; but this remains to be verified.

The normal modes shown in Table 3 are tangent to the intersection-space curvilinear coordinates, f_i (eq 11), and they give a qualitative picture of the motions required to reach a lower energy structure after moving along the conical intersection seam. A more complicated nonlinear combination of normal modes, that is, curvilinear coordinates, would be necessary to trace out a path within the conical intersection seam. Thus, one could not carry out an intrinsic reaction coordinate (IRC) calculation using the displaced modes as starting displacement. Rather, one would either need constraints to remain on the crossing seam or need to use curvilinear coordinates directly.

We now discuss how qualitative dynamics information can be obtained from the analysis of the nature of branching-space

TABLE 4: Dominant Modes Contributing to f_1 (Equation 15), One of the Two Curvilinear Branching-Space Coordinates

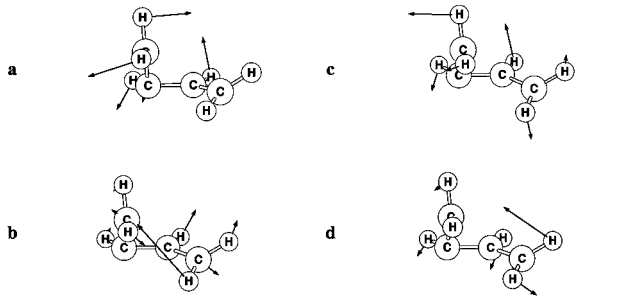

curvilinear coordinates, f_1 (eq 15a) and f_2 (eq 15b). As discussed in the introduction, these coordinates can be used to suggest the normal modes that may be populated at the surface hop. Using the branching-space curvilinear coordinates, f_1 and f_2, the picture given in Figure 1 remains valid; however, the axes become curved (mixtures of the first-order terms gradient difference and derivative coupling with intersection-space coordinates as described in eqs 15a and b). In general, a trajectory passing through a surface hop will have momentum in those coordinates that are populated during evolution on the excited-state reaction path. At the surface hop, additional momentum will be generated in first-order branching-space modes and in those modes that have a large second-order coupling (eq 15), as determined by the eigenvalues of the $\delta\gamma_{ij}$ and η_{ij} matrices. We now discuss this effect for $\mathbf{CI_{cis}}$ butadiene.

At $\mathbf{CI_{cis}}$, the gradient difference and interstate coupling vectors (Table 2) suggest that motions involved in the *s-cis/s-trans* isomerization (Scheme 1a) and cyclobutene closure (Scheme 1d) reaction pathways will be enhanced at the surface hop. With the extension of the definition of the branching space to second order, the modes corresponding to the largest eigenvalues (in absolute value) of the matrix ${}^{IS}\delta\gamma_{ij}$ and ${}^{IS}\eta_{ij}^{AB}$ couple to the branching plane vectors and one might expect such modes to be populated on decay at the conical intersection.

At the $\mathbf{CI_{cis}}$ geometry, there are four (Table 4) large eigenvalues of ${}^{IS}\delta\gamma_{ij}$ (the analysis of ${}^{IS}\eta_{ij}^{AB}$ yields similar conclusions). The mode providing the largest contribution to the f_1 (eq 15a) is shown in Table 4a and corresponds to a methylenic group twisting. Accordingly, after the surface hop the population of this mode is expected to be enhanced and might be expected to contribute to the stimulation of the *Z-E* isomerization pathway (Scheme 1b). The modes reported in Table 4c and d show a similar twisting motion but are primarily localized on the opposite end of butadiene. Thus, momentum will be generated in the *Z,Z-E,E* isomerization coordinate (Scheme 1c). At the same surface hop, one of the coordinates defining the parabolic branching space also has a large component along the mode shown in Table 4b. This motion is parallel to the cyclobutadene formation pathway (Scheme 1d).

In summary, the quadratic definition of branching space around the $\mathbf{CI_{cis}}$ enables one to identify the relevant motions whose population will be enhanced at a surface hop. These modes lie parallel to possible pathways that lead to the formation of four out of the five butadiene photoproducts. However, we emphasize that dynamics studies are necessary to understand whether or not the momentum in the S_1 part of the reaction path predominates over the additional population generated by coupling at the surface hop and also to understand the extent to which the enhancement of the population of these modes at the surface hop is important in the dynamics.

Example 2: The Dynamic Jahn−Teller Effect in the Cyclopentadienyl Radical. In the previous example, the topological structure of the extended conical intersection seam has been characterized by the seam normal modes associated with imaginary frequencies that enable one to interrelate various conical intersection structures. In this last application, we shall study a system showing a dynamic Jahn−Teller effect.[35−36] We discuss this case because a direct connection between the theory of conical intersections presented in this work and spectroscopic experiments is possible.

In the dynamic Jahn−Teller effect, the depth of the moat on the ground-state potential energy surface is so small that the molecule is not localized at the geometry of the global minimum, as in the case of the static Jahn−Teller effect. Thus the Jahn−Teller-Hamiltonian must be evaluated at the central conical intersection geometry in order to rationalize spectroscopic behavior. In this case, the quadratic potential energy matrix proposed in this study (eq 3) can be used to compute both frequencies and normal modes (with the exception of the two "moat" modes) at the Jahn−Teller conical intersection point, as well as all the potential energy constants necessary to fully simulate the recorded emission spectra corrected at the second-order.

The partition of the internal coordinate space proposed in eqs 1 and 2 is a *natural basis* for Jahn−Teller systems: all of the first-order (linear) Jahn−Teller contributions will be confined to the two motions defining the branching plane, which are the only two modes with nonzero first-order contributions (eq 5). In contrast, the analysis of Jahn−Teller systems is usually carried out in special normal coordinates associated with a fictitious minimum at the apex of the cone in Figure 1. However, there are important advantages to the coordinate system defined in eqs 1 and 2. In this case, the two branching-space coordinates can be thought of as linear combinations of all of the so-called *linear Jahn−Teller active modes*, for which the first derivative of the energy evaluated at the conical intersection point is nonzero.[37] Thus, once all the linear contributions to the Hamiltonian are projected out from the Hessian, the $(3N - 8)$ frequencies obtained from the seam analysis are the same as the experimental frequencies.

The preceding analysis makes two assumptions. First, the two vibrational frequencies in the moat of the Jahn−Teller system are excluded from this analysis, but they must be combination of the branching plane vectors (eq 2). However, we have neglected the $\mathbf{W}_a^{(2)}$ (eq 7a) and $\mathbf{W}_c^{(2)}$ (eq 7c), which couple the first-order branching-space modes and the first-order intersection-space modes so this will have some effect on the $(3N - 8)$ intersection-space frequencies. Second, we have assumed that we are in the regime of the dynamic Jahn−Teller effect, that is, the molecule is not localized at the minimum of the moat (*distorted geometry*) and therefore it shows molecular properties of a system lying at the conical intersection geometry (*undistorted geometry*). As we shall show in our analysis of the Jahn−Teller cyclopentadienyl radical, the experimental frequencies are well reproduced.

The cyclopentadienyl radical at D_{5h} geometry has ${}^2E_1''$ electronic symmetry and therefore is subject to Jahn−Teller distortion.[16,19,20,49,50] The conical intersection geometry has been optimized at CASSCF level with a cc-pVDZ basis set, and the geometrical features are summarized in Table S3. Bond lengths and bond angles are in good agreement with the data collected experimentally by means of high-resolution rotational analysis[19−20] and with previously computed values.[20,49] Using symmetry arguments,[16,35] it can be shown that only e_2' modes are able to

TABLE 5: Seam Frequencies (cm^{-1}) Evaluated at the Conical Intersection of Cyclopentadienyl Radical Compared to the Experimental Values

		frequency (cm^{-1})	
mode	symmetry[c]	calculated	experimental[d]
1−2	e_2'	[b]	1041
3−4	e_2''	557	576
5	a_2''	688	684
6−7	e_1''	738	766
8−9	e_2''	853	861
10−11	e_2'	922	872
12−13	e_1'	1064	1001
14	a_1'	1172	1071
15−16	e_2'	1234	1320
17	a_2'	1387	1244
18−19	e_1'	1545	[a]
20−21	e_2'	3374	[a]
22−23	e_1'	3392	[a]
24	a_1'	3408	[a]

[a] Data not reported in ref 19. [b] Frequencies assigned to the gradient difference and nonadiabatic interstate coupling vectors (eq 2). [c] Experimental values taken from ref 19 and references therein. [d] Vibrational symmetries established within D_{5h} point group.

lift linearly the degeneracy between the two states and therefore are linear Jahn−Teller active. The computed gradient difference and interstate coupling vectors indeed transform as e_2' within a D_{5h} point group (Table S4).

The results of the seam frequency analysis are summarized in Table 5. In the third column of this table, we show the frequencies obtained with eq 14 and the frequencies recorded experimentally.[19−20] The two frequencies at 1041 cm^{-1} (third column of Table 5) are assigned to the branching-space vectors. The remaining $(3N - 8)$ frequencies are assigned to the intersection-space modes. The agreement between theory and experiment has an error ranging from 0.5% to 10%, with an average of 2.6% and a standard deviation of 3.1. Certainly the agreement is good enough to confirm the assignment of the spectrum.

In Tables S5 and S6 we give the full set of potential constants for the energy matrix defined in eqs 6 and 8, including the previously neglected terms, $\mathbf{W}_a^{(2)}$ (eq 7a) and $\mathbf{W}_c^{(2)}$ (eq 7c). These potential energy constants could be used in the simulation of experimental spectra. Such potential constants could be obtained routinely for other Jahn−Teller systems, thus providing a more direct comparison between theory and experiment.

5. Conclusions

In this paper, we have presented a theoretical formalism for the quadratic representation of conical intersections. We have shown that the potential constants in such a quadratic representation can be obtained from a state-average Hessian calculation within the CASSCF approach. The analysis of the conical intersection correct to second order involves the definition of curvilinear coordinates (Figure 3), which define the locus of the extended conical intersection seam. Given these curvilinear coordinates, it becomes possible to analyze the curvature of the conical intersection seam energy (minima and saddle points). The more general definition of the branching space in a complementary set of curvilinear coordinates permits one to make some predictions about the dynamics at a conical intersection. Finally, for the special conical intersection associated with the dynamic Jahn−Teller effect, the potential constants permit a direct comparison between theory and experiment.

Application to the extended conical intersection seam associated with the $1A_g/2A_g$ states in butadiene photochemistry shows that this seam is richer than previously documented. In particular, the central conical intersection region has now been shown to be comprised of four different saddle conical intersection points, $^{SP}\mathbf{CI}_{trans/trans}$, $^{SP}\mathbf{CI}_{cis/cis}$, $^{SP}\mathbf{CI}_{cis/trans}$, and $^{SP}\mathbf{CI}_{cis/ring}$. In addition, a new conical intersection, $\mathbf{CI}_{ring}$, has been located along the direction of negative curvature associated with one of the central intersection points, that is, $^{SP}\mathbf{CI}_{cis/ring}$. The analysis of the branching-space curvilinear coordinates at $\mathbf{CI}_{cis}$ suggests that coordinates associated with *Z,Z-E,E* isomerization may be stimulated on decay at the surface hop.

Finally, analysis of the Jahn−Teller system cyclopentadienyl radical shows good agreement between computed and experimental frequencies.

Acknowledgment. L.B. is financed by the Spanish/Ministerio de Educación y Ciencia/ for Project No. CTQ2005-04563 and the Ramón y Cajal program. F.S. is pleased to acknowledge the support of Gaussian, Inc.

Supporting Information Available: Tables S1 and S2 contain the energetics and the linear potential energy constants computed at each optimized butadiene-like conical intersection geometry, respectively. In Table S3, the relevant geometrical features of cyclopentadienyl radical conical intersection are reported. Table S4 contains the gradient difference vector and nonadiabatic interstate coupling vector computed at the cyclopentadienyl radical conical intersection. In Tables S6 and S7, the linear and quadratic potential energy constants computed at the optimized cyclopentadienyl radical conical intersection point are shown. Table S7 contains the Cartesian coordinates for all of the conical intersection structures. This material is available free of charge via the Internet at http://pubs.acs.org.

References and Notes

(1) Migani, A.; Olivucci, M. Conical Intersections and Organic Reaction Mechanisms. In *Conical Intersections: Electronic Structure, Dynamics & Spectroscopy*; Domcke, W., Yarkony, D. R., Koppel, H., Eds.; World Scientific: Singapore, 2004; Vol. 15.

(2) Robb, M. A.; Garavelli, M.; Olivucci, M.; Bernardi, F. A Computational Strategy for Organic Photochemistry. In *Reviews in Computational Chemistry*; Lipkowitz, K. B., Boyd, D.B., Eds.; Wiley-VCH: New York, 2000; Vol. 15.

(3) Zewail, A. H. *J. Phys. Chem. A* **2000**, *104*, 5660.

(4) Olivucci, M.; Robb, M. A.; Bernardi, F. Calculations of Excited State Conformational Properties. In *Conformational Analysis of Molecules in Excited States*; Waluk, J., Ed.; Wiley-VCH: New York, 2000.

(5) Bernardi, F.; Olivucci, M.; Robb, M. A. *Chem. Soc. Rev.* **1996**, 321.

(6) Kessinger, M.; Michl, J. *Excited States and Photochemistry of Organic Molecules*; Wiley-VCH: New York, 1995.

(7) Toniolo, A.; Levine, B.; Thompson, A.; Quenneville, J.; Ben-Nun, M.; Owens, J.; Olsen, S.; Manohar, L.; Martinez, T. J. Photochemistry from First Principles and Direct Dynamics. In *Computational Methods in Organic Photochemistry*; Kutateladze, A., Ed.; Marcel-Dekker: New York, 2005.

(8) Michl, J.; Bonacic-Koutecky, V. *Electronic Aspects of Organic Photochemistry*; Wiley-VCH: New York, 1990.

(9) Yarkony, D. R. Conical Intersections: Their Description and Consequences. In *Conical Intersections: Electronic Structure, Dynamics & Spectroscopy*; Domcke, W., Yarkony, D. R., Koppel, H., Eds.; World Scientific: Singapore, 2004; Vol. 15.

(10) Yarkony, D. R. *Rev. Mod. Phys.* **1996**, *68*, 985.

(11) Koppel, H.; Domcke, W.; Cederbaum, L. S. The Multi-Mode Vibronic Coupling Approach. In *Conical Intersections: Electronic Structure, Dynamics & Spectroscopy*; Domcke, W., Yarkony, D. R., Koppel, H., Eds.; World Scientific: Singapore, 2004; Vol. 15.

(12) Worth, G. A.; Meyer, H. D.; Cederbaum, L. S. Multidimensional Dynamics Involving a Conical Intersection: Wavepacket Calculations Using the MCTDH Method. In *Conical Intersections: Electronic Structure, Dynamics & Spectroscopy*; Domcke, W., Yarkony, D. R., Koppel, H., Eds.; World Scientific: Singapore, 2004; Vol. 15.

(13) Jasper, A. W.; Kendrick, B. K.; Mead, C. A.; Truhlar, D. G. Non-Born-Oppenheimer Chemistry: Potential Surfaces, Couplings, and Dynamics. In *Modern Trends in Chemical Reaction Dynamics: Experiments and Theory (Part 1)*; Yang, X., Liu, K., Eds.; World Scientific: Singapore, 2004.
(14) Bernardi, F.; Olivucci, M.; Michl, J.; Robb, M. A. *The Spectrum* **1996**, *9*, 16.
(15) Paterson, M. J.; Bearpark, M. J.; Robb, M. A.; Blancafort, L. *J. Chem. Phys.* **2004**, *121*, 11562.
(16) Paterson, M. J.; Bearpark, M. J.; Robb, M. A.; Blancafort, L.; Worth, G. A. *Phys. Chem. Chem. Phys.* **2005**, *7*, 2100.
(17) Yarkony, D. R. *J. Chem. Phys.* **2005**, *123*, 134106.
(18) Yarkony, D. R. *J. Chem. Phys.* **2005**, *123*, 204101.
(19) Applegate, B. E.; Bezant, A. J.; Miller, T. A. *J. Chem. Phys.* **2001**, *114*, 4869.
(20) Applegate, B. E.; Miller, T. A.; Barckholtz, T. A. *J. Chem. Phys.* **2001**, *114*, 4855.
(21) Miller, T. A. Holding Computations of Conical Intersections to a Gold Standard. In *Quantum Dynamics at Conical Intersections*; Worth, G. A., Althorpe, S. C., Eds.; Collaborative computational project on molecular quantum dynamics (CCP6), Daresbury, 2004.
(22) Koppel, H.; Domcke, W.; Cederbaum, L. S. *Adv. Chem. Phys.* **1984**, *57*, 59.
(23) Mead, C. A. *J. Chem. Phys.* **1983**, *78*, 807.
(24) Atchity, G. J.; Xantheas, S. S.; Ruedenberg, K. *J. Chem. Phys.* **1991**, *95*, 1862.
(25) Ragazos, I. N.; Robb, M. A.; Bernardi, F.; Olivucci, M. *Chem. Phys. Lett.* **1992**, *197*, 217.
(26) Yarkony, D. R. Determination of Potential Energy Surface Intersections and Derivative Couplings in the Adiabatic Representation. In *Conical Intersections: Electronic Structure, Dynamics & Spectroscopy*; Domcke, W., Yarkony, D. R., Koppel, H., Eds.; World Scientific: Singapore, 2004; Vol. 15.
(27) Boggio-Pasqua, M.; Ravaglia, M.; Bearpark, M. J.; Garavelli, M.; Robb, M. A. *J. Phys. Chem. A* **2003**, *107*, 11139.
(28) Boggio-Pasqua, M.; Bearpark, M. J.; Ogliaro, F.; Robb, M. A. *J. Am. Chem. Soc.* **2006**, *128*, 10537.
(29) Garavelli, M. *Theor. Chem. Acc.* **2006**, *116*, 87.
(30) Toniolo, A.; Ben-Nun, M.; Martinez, T. J. *J. Phys. Chem. A* **2002**, *106*, 4679.
(31) Serrano-Andres, L.; Merchan, M.; Lindh, R. *J. Chem. Phys.* **2005**, *122*, 104107.
(32) Bearpark, M. J.; Robb, M. A.; Schlegel, H. B. *Chem. Phys. Lett.* **1994**, *223*, 269.
(33) Lee, T. J.; Fox, D. J.; Schaeffer, H. F., III; Pitzer, R. M. *J. Chem. Phys.* **1984**, *81*, 356.
(34) Desouter-Lecomte, M.; Galloy, C.; Lorquet, J. C.; Vaz Pires, M. *J. Chem. Phys.* **1979**, *71*, 3661.
(35) Bersuker, I. B. *The Jahn-Teller Effect*; Cambridge University Press: Cambridge, 2006.
(36) Barckholtz, T. A.; Miller, T. A. *J. Phys. Chem. A* **1999**, *103*, 2321.
(37) Applegate, B. E.; Barckholtz, T. A.; Miller, T. A. *Chem. Soc. Rev.* **2003**, *32*, 38.
(38) Koppel, H.; Domcke, W.; Cederbaum, L. S. *Adv. Chem. Phys.* **1984**, *57*, 59.
(39) Davidson, E. R. *J. Am. Chem. Soc.* **1977**, *99*, 397.
(40) Yamamoto, N.; Vreven, T.; Robb, M. A.; Frisch, M. J.; Schlegel, B. H. *Chem. Phys. Lett.* **1996**, *250*, 373.
(41) Vreven, T. The Theoretical Investigation of Photochemical Reactions: Ab Initio Trajectories with Surface Hopping. Ph.D. Thesis, University of London, 1998.
(42) Byron, F. W.; Fuller, R. W. *Mathematics of Classical and Quantum Physics*; Dover Publications, New York, 1969.
(43) Frisch, M. J.; Trucks, G. W.; Schlegel, H. B.; Scuseria, G. E.; Robb, M. A.; Cheeseman, J. R.; Montgomery, J. A., Jr.; Vreven, T.; Scalmani, G.; Kudin, K. N.; Iyengar, S. S.; Tomasi, J.; Barone, V.; Mennucci, B.; Cossi, M.; Rega, N.; Petersson, G. A.; Nakatsuji, H.; Hada, M.; Ehara, M.; Toyota, K.; Fukuda, R.; Hasegawa, J.; Ishida, M.; Nakajima, T.; Honda, Y.; Kitao, O.; Nakai, H.; Li, X.; Hratchian, H. P.; Peralta, J. E.; Izmaylov, A. F.; Brothers, E.; Staroverov, V.; Kobayashi, R.; Normand, J.; Burant, J. C.; Millam, J. M.; Klene, M.; Knox, J. E.; Cross, J. B.; Bakken, V.; Adamo, C.; Jaramillo, J.; Gomperts, R.; Stratmann, R. E.; Yazyev, O.; Austin, A. J.; Cammi, R.; Pomelli, C.; Ochterski, J. W.; Ayala, P. Y.; Morokuma, K.; Voth, G. A.; Salvador, P.; Dannenberg, J. J.; Zakrzewski, V. G.; Dapprich, S.; Daniels, A. D.; Strain, M. C.; Farkas, O.; Malick, D. K.; Rabuck, A. D.; Raghavachari, K.; Foresman, J. B.; Ortiz, J. V.; Cui, Q.; Baboul, A. G.; Clifford, S.; Cioslowski, J.; Stefanov, B. B.; Liu, G.; Liashenko, A.; Piskorz, P.; Komaromi, I.; Martin, R. L.; Fox, D. J.; Keith, T.; Al-Laham, M. A.; Peng, C. Y.; Nanayakkara, A.; Challacombe, M.; Chen, W.; Wong, M. W.; Pople, J. A. *Gaussian DV*, revision E.05; Gaussian, Inc.: Wallingford, CT, 2006.
(44) Squillacote, M.; Semple, T. C. *J. Am. Chem. Soc.* **1990**, *112*, 5546.
(45) Celani, P.; Bernardi, F.; Olivucci, M.; Robb, M. A. *J. Chem. Phys.* **1995**, *102*, 5733.
(46) Olivucci, M.; Ragazos, I. N.; Bernardi, F.; Robb, M. A. *J. Am. Chem. Soc.* **1993**, *115*, 3710.
(47) Garavelli, M.; Bernardi, F.; Olivucci, M.; Bearpark, M. J.; Klein, S.; Robb, M. A. *J. Phys. Chem. A* **2001**, *105*, 11496.
(48) Garavelli, M.; Frabboni, B.; Fato, M.; Celani, P.; Bernardi, F.; Robb, M. A.; Olivucci, M. *J. Am. Chem. Soc.* **1999**, *121*, *1537*.
(49) Bearpark, M. J.; Robb, M. A.; Yamamoto, N. *Spectrochim. Acta, Part A* **1999**, *55*, 639.
(50) (a) Borden, W. T.; Davidson, E. R. *J. Am. Chem. Soc.* **1979**, *101*, 3771. (b) Yu, L.; Foster, S. C.; Williamson, J. M.; Heaven, M. C.; Miller, T. A. *J. Phys. Chem.* **1988**, *92*, 4263.